TOWARDS A MORE RELIABLE ESTIMATION OF FOREST PARAMETERS FROM POLARIMETRIC SAR TOMOGRAPHY DATA

Othmar Frey
Earth Observation & Remote Sensing
ETH Zurich, Switzerland /
Gamma Remote Sensing,
Switzerland
Email: otfrey@ethz.ch

Erich Meier
Remote Sensing Laboratories
University of Zurich
Switzerland

Irena Hajnsek
Earth Observation & Remote Sensing
ETH Zurich, Switzerland /
German Aerospace Center - DLR,
Germany

***Abstract*—In this contribution, tomographic imagery obtained from estimating the 3-D localization and the polarimetric signature of backscattering sources within a forest environment from fully-polarimetric multibaseline SAR data at L- and P-bands are presented. Both, polarization diversity and spatial diversity were exploited jointly within the tomographic focusing to estimate the targets' localization and polarimetric signature. We thereby extend our recently proposed time-domain back-projection (TDBP)-based tomographic focusing approach. The tomographic slices obtained from polarimetric spectral estimation using MLBF, Capon, and MUSIC are opposed to the results previously obtained by tomographic focusing of the individual polarization channels. The results are briefly discussed with respect to potential advancements towards more reliable estimation of forest parameters from SAR tomography data.**

***Index Terms*—SAR tomography, beamforming, Capon, MUSIC, forestry**

I. Introduction

Various SAR tomography concepts to retrieve structural information of forest volumes were proposed and demonstrated in a number of experiments during the last couple of years [1]–[13]. In this paper, we determine the localization and the polarimetric signature of backscattering sources within a forest environment by jointly using the different polarization channels in the tomographic focusing process thereby extending our time-domain back-projection (TDBP)-based tomographic focusing approaches described in [12], where the individual polarization channels were estimated individually. The respective results are compared and discussed.

II. Data

The experimental data consists of the two SAR tomography data sets that were also used in our previous work on tomography-based characterization of a forest [5], [6], [12], [13]. This ensures a good comparability of the performance of the various single- and fully-polarimetric tomographic processing methods. Both tomographic data sets, at L- and P-bands, are fully polarimetric. The data was acquired by the German Aerospace Center's E-SAR sensor over a partially forested area in Switzerland. A detailed description of the experimental setup is found in [13]. The most important parameters regarding sensor specifications and tomographic acquisition geometry are reproduced in Table I.

TABLE I
E-SAR system specifications and nominal parameters of the tomographic acquisition patterns for both multibaseline data sets at P-band and L-band.

	P-band	**L-band**
Carrier frequency	350 MHz	1.3 GHz
Chirp bandwidth	70 MHz	94 MHz
Sampling rate	100 MHz	100 MHz
PRF	500 Hz	400 Hz
Ground speed	90 m/s	90 m/s
No. of data tracks	11+1	16+1
Nominal track spacing d_n	57 m	14 m
Horizontal baselines	40 m	10 m
Vertical baselines	40 m	10 m
Synthetic aperture in normal direction L	570 m	210 m
Nominal resolution in normal direction δ_n	3 m	2 m
Approx. unambiguous height H	30 m	30 m

III. Methods

The time-domain back-projection (TDBP-)based single channel focusing approaches used here for compar-

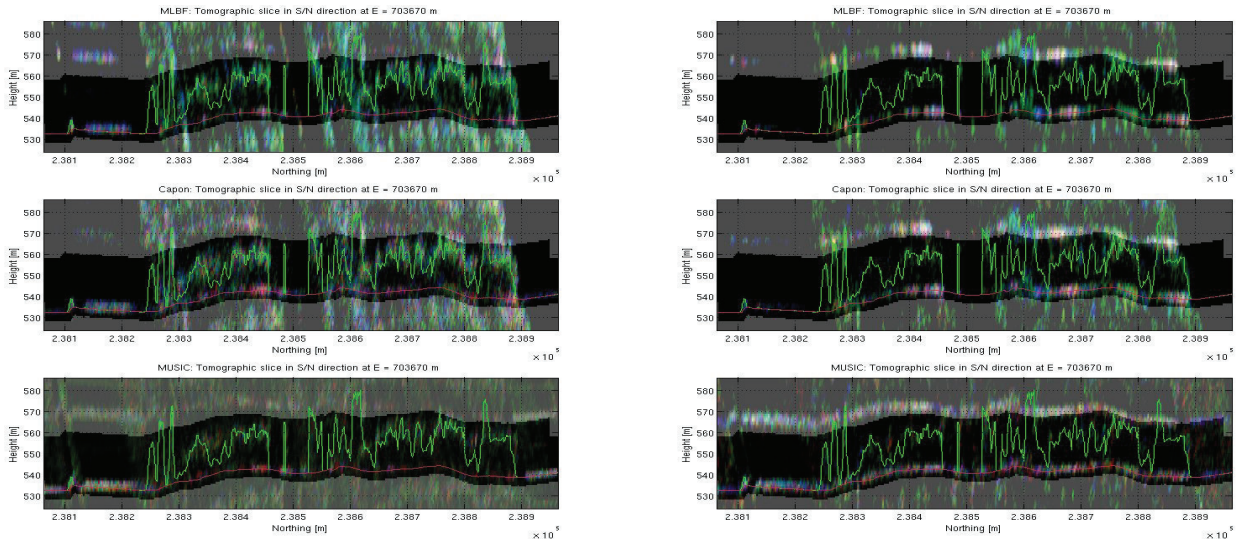

(a) (b)

Fig. 1. Vertical slices through a 3-D volume of a forested area obtained from multibaseline (a) L-Band and (b) P-band data set using all (16, and 11) repeat-pass tracks. Red (HH), green (HV), blue (VV). Each channel has been focused and scaled individually. Greyed areas indicate ambiguous target regions. The tomographic slices run in south-northern direction (at easting coordinate E = 703670 m) and are overlaid by the DEM (solid red line) and the DSM (solid green line) from ALS. Top: MLBF, middle: RCB, bottom: MUSIC. The above tomographic slices were originally published in [12] and are reproduced here for comparison.

ison are described in [12] and an even more extended description is found in [14]. In the following, only the main steps of the joint polarimetric-multibaseline SAR focusing are sketched for (1) polarimetric multilook beamforming, (2) polarimetric multiple signal classification (MUSIC), and (3) polarimetric Capon beamforming. A more detailed treatment of these joint polarimetric-multibaseline spectral estimation approaches is found in e.g. [15], [16], and such approaches were recently applied in the context of building height estimation by polarimetric multibaseline SAR [17] as well as for forest scenarios [10].

The steering vector $\mathbf{a}(z)$, as a function of height z, for one polarization channel is:

$$\mathbf{a}(z) = [1 \; e^{i\varphi_2(z)} \dots e^{i\varphi_K(z)}]^T \; , \tag{1}$$

where $\varphi_m = -2k_c(r_m - r_1)$, $m = 1 \dots K$. k_c is the central wavenumber and r_m is the range distance from the backscattering element to the m-th sensor position. For polarimetric focusing, the data vectors of the different polarization channels $\mathbf{y}_{p_1} \dots \mathbf{y}_{p_4}$ are subsequently aligned within the signal vector $\mathbf{y}$ (shown here for 4 polarization channels $(p1, \dots, p_4)$):

$$\mathbf{y}(z) = [y_{1_{p_1}}(z) \dots y_{K_{p_1}}(z) \dots\dots y_{1_{p_4}}(z) \dots y_{K_{p_4}}(z)]^T \; . \tag{2}$$

The polarimetric data vector for each look $l = 1, \dots, N$ can then be stored conveniently in the data matrix $\mathbf{Y}$ using the following matrix structure:

$$\mathbf{Y} = [\mathbf{y}_1 \; \mathbf{y}_2 \dots \mathbf{y}_N] \; , \tag{3}$$

such that the sample covariance matrix can be written as

$$\hat{\mathbf{R}} = \frac{1}{N}\mathbf{Y}\mathbf{Y}^H \; . \tag{4}$$

In contrast to the single polarization case the steering vectors $\mathbf{a}$ are filled into a steering matrix $\mathbf{A}$ according to the data alignment as employed in $\mathbf{y}$:

$$\mathbf{A} = \begin{bmatrix} \mathbf{a} & 0 & 0 & 0 \\ 0 & \mathbf{a} & 0 & 0 \\ 0 & 0 & \mathbf{a} & 0 \\ 0 & 0 & 0 & \mathbf{a} \end{bmatrix} \tag{5}$$

The estimation procedures for the different focusing techniques are as follows:

a) Polarimetric MLBF: (1) Eigenvalue decomposition of $(\mathbf{A}^H\hat{\mathbf{R}}\mathbf{A}) = \mathbf{U}\mathbf{\Gamma}\mathbf{U}^H$. (2) Extract the maximum eigenvalue λ_{max} and its corresponding eigenvector $u_{\lambda_{max}}$. (3) The total power of the MLBF-focused tomographic signal is then given as: $P_B = \lambda_{max}/p^2$, where p is the total number of channels (polarimetric *and* spatial separation).

b) Polarimetric Capon: (1) Eigenvalue decomposition of $(\mathbf{A}^H\hat{\mathbf{R}}^{-1}\mathbf{A}) = \mathbf{U}\mathbf{\Gamma}\mathbf{U}^H$. (2) Extract the mini-

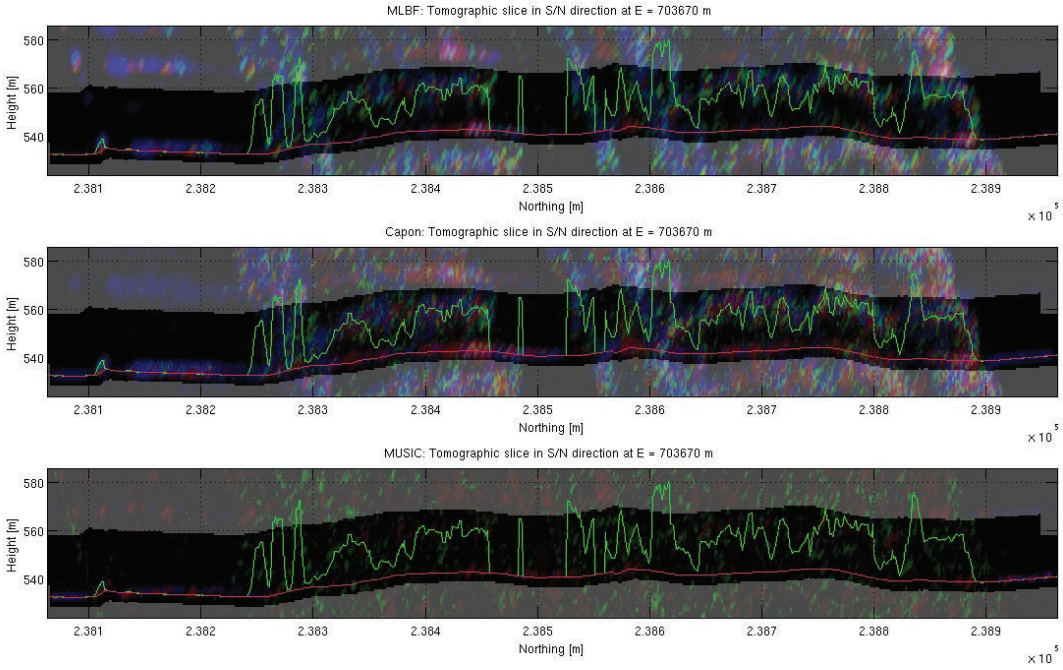

(a)

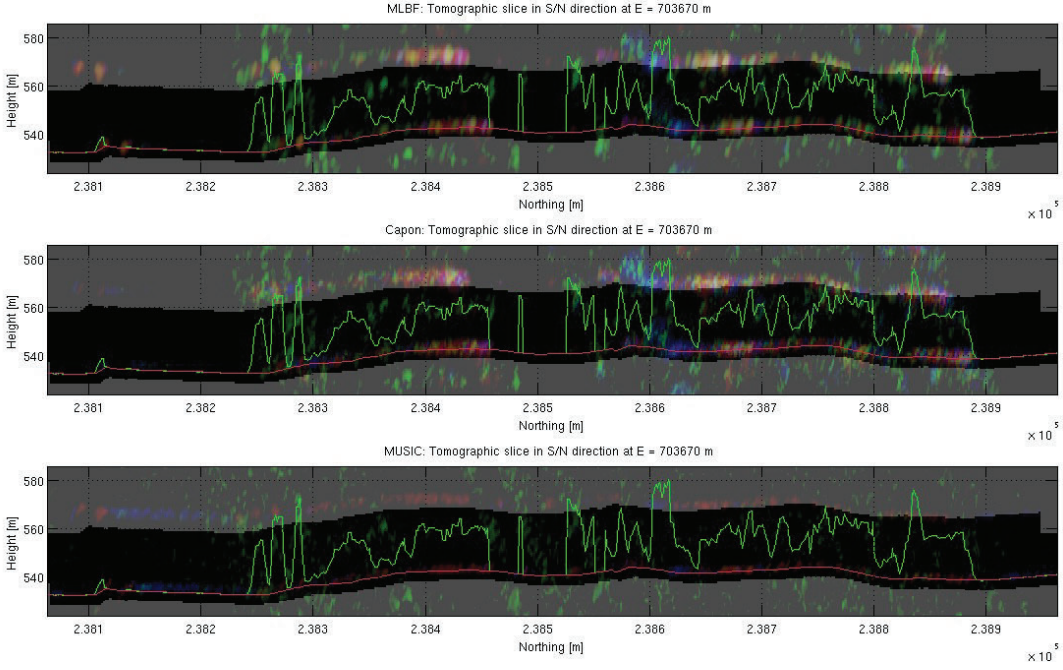

(b)

Fig. 2. Vertical slices through a 3-D volume of a forested area obtained from polarimetric multibaseline (a) L-Band and (b) P-band data set using all (16, and 11) repeat-pass tracks. Red (HH), green (HV), blue (VV). Joint polarimetric-multibaseline tomographic focusing. Greyed areas indicate ambiguous target regions. The tomographic slices run in south-northern direction (at easting coordinate E = 703670 m) and are overlaid by the DEM (solid red line) and the DSM (solid green line) from ALS. Top: polarimetric MLBF, middle: polarimetric Capon, bottom: polarimetric MUSIC.

mum eigenvalue λ_{min} and its corresponding eigenvector $u_{\lambda_{min}}$. (3) The Capon spectral estimate is then obtained as $P_c = 1/\lambda_{min}$.

c) Polarimetric MUSIC: (1) Eigenvalue decomposition of the sample covariance matrix $\hat{\mathbf{R}}$, and subsequent extraction of its noise-subspace $\mathbf{G}$. (2) Eigenvalue de-

composition of $(\mathbf{A}^H\mathbf{G}\mathbf{G}^H\mathbf{A}) = \mathbf{U}\mathbf{\Gamma}\mathbf{U}^H$. (3) Extract the minimum eigenvalue λ_{min} and the eigenvector $u_{\lambda_{min}}$. (4) The MUSIC pseudo-spectrum is then: $P_{mu} = 1/\lambda_{min}$.

IV. Results

In Fig. 1 vertical tomographic slices in south-northern direction are given for the case where all polarization channels were focused individually using MLBF, RCB, and MUSIC. These tomographic slices were originally published in [12] and are reproduced here for comparison. In Fig. 2 the respective vertical tomographic slices are shown for the joint polarimetric-multibaseline tomographic focusing using polarimetric MLBF, polarimetric Capon, and polarimetric MUSIC.

V. Discussion

The results of the comparison obtained so far indicate that a joint exploitation of polarization and baseline diversity at the step of tomographic imaging is beneficial in the sense that it leads to less biased estimates of the main scattering locations in many cases since at each potential source location the optimal polarization state can be extracted. A joint combination of polarization and baseline diversity also provides a way to better maintain polarization information throughout the tomographic focusing step not only in the beamforming case (as shown in [13]) but also when using more advanced spectral estimation methods, such as the Capon spectral estimators. MUSIC seems to behave unstable depending on the target structure; a major problem in this case is the a priori selection of the model order. In general, a trade-off has to be made with regard to a higher amount of multilooking that is required to obtain stable solutions for the fully-polarimetric tomographic focusing. Thereby the resolution in the (ground-)range-azimuth domain is reduced leading to a loss of smaller features. Potentially interesting features, such as gaps in the canopy, variation of the height of the canopy are averaged out to a considerable extent, or might even be lost completely.

Acknowledgment

The authors would like to thank the procurement and technology center of the Swiss Federal Department of Defense (armasuisse W+T) for supporting this work. They would also like to thank the E-SAR/F-SAR team at the Department of SAR Technology, German Aerospace Center (DLR) for their ongoing cooperation.

References

[1] A. Reigber and A. Moreira, "First Demonstration of Airborne SAR Tomography Using Multibaseline L-Band Data," *IEEE Transactions on Geoscience and Remote Sensing*, vol. 38, no. 5, pp. 2142–2152, 2000.

[2] F. Lombardini and A. Reigber, "Adaptive spectral estimation for multibaseline SAR tomography with airborne L-band data," in *IEEE International Geoscience and Remote Sensing Symposium, IGARSS '03.*, vol. 3, 2003, pp. 2014–2016.

[3] A. Reigber, M. Neumann, S. Guillaso, S. Sauer, and L. Ferro-Famil, "Evaluating PolInSAR parameter estimation using tomographic imaging results," in *Proc. European Radar Conf.*, 2005, pp. 189–192.

[4] M. Nannini and R. Scheiber, "A time domain beamforming algorithm for sar tomography," in *Proc. of EUSAR 2006 - 6th European Conference on Synthetic Aperture Radar*, 2006.

[5] O. Frey, F. Morsdorf, and E. Meier, "Tomographic Processing of Multi-Baseline P-Band SAR Data for Imaging of a Forested Area," in *Proc. IEEE Int. Geosci. Remote Sens. Symp.*, 2007.

[6] O. Frey, F. Morsdorf, and E. Meier, "Tomographic Imaging of a Forested Area By Airborne Multi-Baseline P-Band SAR," *Sensors, Special Issue on Synthetic Aperture Radar*, vol. 8, no. 9, pp. 5884–5896, sep 2008.

[7] M. Nannini, R. Scheiber, and A. Moreira, "Estimation of the minimum number of tracks for SAR tomography," *IEEE Trans. Geosci. Remote Sens.*, vol. 47, no. 2, pp. 531–543, Feb. 2009.

[8] S. Tebaldini, "Algebraic synthesis of forest scenarios from multibaseline PolInSAR data," *IEEE Trans. Geosci. Remote Sens.*, vol. 47, no. 12, pp. 4132–4142, Dec. 2009.

[9] F. Lombardini, F. Cai, and M. Pardini, "Tomographic analyses of non-stationary volumetric scattering," in *Proc. EUSAR*, June 2010, pp. 1–4.

[10] Y. Huang, L. Ferro-Famil, and A. Reigber, "Under foliage object imaging using SAR tomography and polarimetric spectral estimators," in *Proc. EUSAR*, June 2010, pp. 1–4.

[11] S. Tebaldini, "Single and multipolarimetric SAR tomography of forested areas: A parametric approach," *IEEE Trans. Geosci. Remote Sens.*, vol. 48, no. 5, pp. 2375–2387, May 2010.

[12] O. Frey and E. Meier, "3-D time-domain SAR imaging of a forest using airborne multibaseline data at L- and P-bands," *IEEE Trans. Geosci. Remote Sens.*, vol. 49, no. 10, pp. 3660–3664, Oct. 2011.

[13] O. Frey and E. Meier, "Analyzing tomographic SAR data of a forest with respect to frequency, polarization, and focusing technique," *IEEE Trans. Geosci. Remote Sens.*, vol. 49, no. 10, pp. 3648–3659, Oct. 2011.

[14] O. Frey, *Synthetic Aperture Radar Imaging in the Time Domain for Nonlinear Sensor Trajectories and SAR Tomography*, ser. PhD Thesis. Remote Sensing Series, vol. 59, Remote Sensing Laboratories, University of Zurich, Zurich, Switzerland, 2010. ISBN: 978-3-03703-025-7.

[15] R. O. Schmidt, "Multiple emitter location and signal parameter estimation," *IEEE Transactions on Antennas and Propagation*, vol. 34, no. 3, pp. 276–280, Mar 1986.

[16] E. R. Ferrara and T. M. Parks, "Direction finding with an array of antennas having diverse polarizations," *IEEE Transactions on Antennas and Propagation*, vol. 31, no. 2, pp. 231–236, Mar. 1983.

[17] S. Sauer, L. Ferro-Famil, A. Reigber, and E. Pottier, "Polarimetric dual-baseline InSAR building height estimation at L-band," *IEEE Geoscience and Remote Sensing Letters*, vol. 6, no. 3, pp. 408–412, July 2009.